Computational Thermal Sciences, 12(5):401–415 (2020)

NUMERICAL AND EXPERIMENTAL MODELING OF LYOPHILIZATION OF LACTOSE AND MANNITOL WATER SOLUTIONS IN VIALS

M. Ramšak,[1] M. Zadravec,[1] J. Ravnik,[1] J. Iljaž,[1] M. Avanzo,[2] K. Kočevar,[2] Š. Irman,[2] M. Cegnar,[2] I. Golobič,[3] A. Sitar,[3] & M. Hriberšek[1,]*

[1]*Faculty of Mechanical Engineering, University of Maribor, Smetanova ulica 17, SI-2000 Maribor, Slovenia*

[2]*LEK d.d., Verovškova 57, SI-1526 Ljubljana, Slovenia*

[3]*Faculty of Mechanical Engineering, University of Ljubljana, Aškerčeva cesta 6, SI-1000 Ljubljana, Slovenia*

*Address all correspondence to: M. Hriberšek, Faculty of Mechanical Engineering, University of Maribor, Smetanova ulica 17, SI-2000 Maribor, Slovenia, E-mail: matjaz.hribersek@um.si

The paper reports on the development of a numerical model for the simulation of a lyophilization process in a vial. Lactose and mannitol-water mixtures are used as the working media. Experimental analysis of the lyophilization dynamics inside a single vial in a laboratory scale lyophilizer is reported, with the main focus on the primary drying phase. In order to assess the primary drying kinetics, the temperature distribution along the vertical axis of the samples is measured. In the numerical model, a one-dimensional (1D) vial approximation is used, and governing equations of the heat and water vapor transport with moving front between the frozen and the porous part of the filling are solved by a finite difference method in a time stepping nonlinear iteration procedure. A dedicated mapping of heat transfer boundary conditions, derived for the axisymmetric vial case, is applied for the case of the 1D vial geometry approximation. The main difference in the drying of lactose and mannitol solutions lies in the fact that the lactose shows undercooling effects during the primary drying phase, which is not the case for the mannitol solution. This effect is a consequence of shrinking behavior of the lactose porous cake, leading to a loss of contact with the vial side and hence to a decrease in the overall heat input to the vial. In order to account for the shrinking process in the numerical model, a linear approximation of the decrease of the heat transfer from the vial side wall during the simulation is introduced. The comparison of the numerical and experimental results shows that the developed numerical model is able to accurately capture the movement of the sublimation front, dividing the frozen from the porous part of the filling, at typical locations inside the vial, accompanied also by an accurate capturing of the temperature levels inside the drying material, with the derived numerical model also able to reproduce the temperature drop during the primary drying of the lactose solution.

KEY WORDS: *lyophilization, freeze-drying, vial, heat and mass transfer, finite difference method, sublimation, mannitol, lactose*

1. INTRODUCTION

Lyophilization is one of the most time and energy consuming separation processes, used in the pharmaceutical industry. It is based on drying in form of a direct phase change of a frozen solvent into a gaseous state; therefore, it is characterized by low temperature levels and extremely low system pressures in the order of 10 Pa. Because the lyophilization is performed at relatively low temperatures, the base material is preserved with all its quality, which is the reason why the lyophilization is mostly used in the food, chemical, pharmaceutical, and biotechnology industries (Cornu et al., 2000; Gan et al., 2004; Sheehan and Liapis, 1998). In the food industry, the product is usually placed freely on the trays, whereas in the pharmaceutical industry the product (solution) is predominantly filled in vials.

NOMENCLATURE

$c_{p,1}$	effective specific heat [J/kg] for the porous region
$c_{p,2}$	effective specific heat [J/kg] for the frozen region
$c_{p,g}$	specific heat [J/kg] for a mixture of water vapor and inert gas
ρ_1	effective density [kg/m^3] of the porous region
ρ_2	effective density [kg/m^3] of the frozen region
$\rho_{1,p}$	density [kg/m^3] of porous cake in Region 1
ΔH_v	enthalpy of vaporization [J/kg]
ΔH_s	enthalpy of sublimation [J/kg]
λ_1	thermal conductivity [W/m K] of the porous region
λ_2	thermal conductivity [W/m K] of the frozen region
λ_{gas}	thermal conductivity [W/m K] of gas
$\vec{N}_v$	mass flux [kg/m^{2}s] of water vapor in porous region
$\vec{N}_i$	mass flux [kg/m^{2}s] of inert gas in porous region
C	concentration of adsorbed water in porous region [kg/kg]
$C^\star$	equilibrium concentration of adsorbed water in porous region [kg/kg]
v_n	speed of movement of the sublimation front [m/s]
$N_{v,n}$	normal mass flux [kg/m^{2}s] of water vapor in porous region
k_g	water desorption rate [s^{-1}]
ϵ	porosity of the cake in Region 1 [–]
ϵ_{glass}	emissivity of glass [–]
ϵ_{shelf}	emissivity of shelf [–]
M_v	molecular weight of water [kg/kmol]
M_i	molecular weight of inert gas [kg/kmol]
R	ideal gas constant [8314 J/kmol K]
p_v	partial water vapor pressure in Region 1 [Pa]
p_i	partial inert gas pressure in Region 1 [Pa]
p_c	system pressure [Pa]
$p_v^\star$	equilibrium partial water vapor pressure at sublimation front [Pa]
T	temperature [K]
T_{shelf}	shelf temperature [K]
T_{bot}	glass temperature at the bottom of the vial [K]
T_{top}	temperature at the top of the porous region [K]
t	time [s]
C_{01}	model parameter for relative Darcy flow permeability [–]
C_1	model parameter for relative Knudsen flow permeability [m]
C_2	ratio of bulk diffusivity in the porous medium to free gas bulk diffusivity [–]
$D_{v,i}$	diffusivity of a binary mixture of water vapor and inert gas [m^2/s]
K_{vo}	equivalent heat transfer coefficient [W/m K]
K_{vt}	equivalent heat transfer coefficient at the top of domain [W/m K]
K_{vs}	equivalent heat transfer coefficient at the side of domain [W/m K]
K_{vb}	equivalent heat transfer coefficient at the bottom of domain [W/m K]
K_{vc}	equivalent contact conduction heat transfer coefficient [W/m K]
K_v	Knudsen diffusivity for water vapor [m^2/s]
K_i	Knudsen diffusivity for inert gas [m^2/s]
K_{mx}	Knudsen diffusivity for a mixture of water vapor and inert gas [m^2/s]
μ_{mx}	viscosity of mixture of water vapor and inert gas [kg/ms]
k_1, k_3	bulk diffusivity constant
k_2, k_4	self diffusivity constant
σ	the Stefan–Boltzmann constant
α_c	accommodation coefficient [–]
F_{12}	view factor
h_{fill}	height of the vial filling [m]
l	integral conduction length [m]
$\dot{m}_v$	water vapor mass flux [g/h]
R_p	mass transfer resistance [cm^2 torr h/g]

In order to better understand the scale-up process in lyophilization, extensive research has been invested into the derivation of advanced theoretical (Kasper et al., 2013; Pikal et al., 1984), and computational models (Mascarenhas et al., 1997; Song and Nam, 2005), to name just a few. The advanced models typically rely on using partial differential equations (PDE) of heat and mass transfer (Sadikoglu and Liapis, 1997), including the sorption and sublimation models (Mascarenhas et al., 1997; Song and Nam, 2005). In Mascarenhas et al. (1997) the lyophilization model was solved using the finite element method (FEM) with arbitrary Lagrangian–Eulerian (ALE) scheme, and Song and Nam (2005) developed the finite volume method based model to solve the mathematical model described by Sheehan and Liapis (1998) to solve the problem of skim milk freeze-drying in a vial. Recently, the development of computational models for the case of the vial was extended to the computational determination of the design space (Giordano et al., 2011) and to including the derived vial models into a general computational fluid dynamics framework, with vial models serving as the heat and mass transfer sinks and sources (Zhu et al., 2018). In both latter cases, the core of the predictive computational model is the lyophilization model for a single vial, which first needs to account for all the phenomena, that determine the lyophilization dynamics, and second is computationally effective in order to allow reasonably fast calculation of various lyophilization cases. The latter is also the reason for the need for further development of one-dimensional (1D) geometrical models of lyophilization, which should include all the relevant physics that influence the validity of the models.

In the present work, a numerical model, based on the finite difference method, of the conjugate heat and mass transfer problem in a 1D approximation of a vial filling that is able to reproduce the effect of the porous cake shrinking on the lyophilization dynamics, is presented, together with a comparison to experimental results. The influence of different physical behavior of drying solutions, lactose and mannitol water solutions in our case, on drying characteristics is discussed, especially in connection with the numerical solution of the governing equations.

2. COMPUTATIONAL MODEL

Lyophilization is a heat and mass transfer problem with a moving interface, separating the frozen part (denoted by 2) from the porous part (denoted by 1) with no ice. In the porous domain, we have a conjugate heat and mass transfer problem, and in the frozen part, the process is driven by heat transfer only. In the frozen part of the solution, heat transfer is governed by the conduction process only and the conservation of energy for the frozen part reads as

$$\underbrace{\rho_2 c_{p,2}\frac{\partial T}{\partial t}}_{accumulation} = \underbrace{\lambda_2 \nabla^2 T}_{diffusion}. \tag{1}$$

In the porous region, heat transfer is governed by convection and conduction, and the desorption process gives rise to the heat source:

$$\underbrace{\rho_1 c_{p,1}\frac{\partial T}{\partial t}}_{accumulation} + \underbrace{\vec{\nabla}\cdot\left((\vec{N_v}+\vec{N_i})c_{p,g}T\right)}_{convection} = \underbrace{\lambda_1\nabla^2 T}_{diffusion} + \underbrace{\Delta H_v \rho_{1,p}\frac{\partial C}{\partial t}}_{desorption}. \tag{2}$$

At the sublimation front, separating the frozen from the porous part of the domain, the following compatibility condition must be satisfied:

$$\lambda_2\frac{\partial T}{\partial n}\bigg|_2 + \underbrace{v_n\rho_2 c_{p,2}T}_{interface\ term} = \lambda_1\frac{\partial T}{\partial n}\bigg|_1 + \underbrace{v_n\rho_1 c_{p,1}T}_{interface\ term} - \underbrace{\Delta H_s N_{v,n}}_{sublimation} - \underbrace{N_{v,n}c_{p,g}T|_1}_{convection} \tag{3}$$

with v_n being the normal velocity of the interface,

$$v_n = -\frac{N_{v,n}}{\rho_2 - \rho_1}. \tag{4}$$

Mass conservation is computed only for the porous part, where the inert gas and water vapor are present. For water vapor, the conservation of mass reads as

$$\underbrace{\epsilon \frac{M_v}{R}\frac{\partial}{\partial t}\left(\frac{p_v}{T}\right)}_{accumulation} + \underbrace{\vec{\nabla}\cdot\vec{N_v}}_{convection} = -\underbrace{\rho_{1,p}\frac{\partial C}{\partial t}}_{desorption}, \tag{5}$$

and for the inert gas it is as follows:

$$\underbrace{\epsilon \frac{M_i}{R}\frac{\partial}{\partial t}\left(\frac{p_i}{T}\right)}_{accumulation} + \underbrace{\vec{\nabla}\cdot\vec{N_i}}_{convection} = 0. \tag{6}$$

Mass fluxes of the water vapor and the inert gas are computed as follows:

$$\vec{N_v} = -\frac{M_v}{RT}[k_1\vec{\nabla}p_v + k_2 p_v(\vec{\nabla}p_v + \vec{\nabla}p_i)], \tag{7}$$

$$\vec{N_i} = -\frac{M_i}{RT}[k_3\vec{\nabla}p_i + k_4 p_i(\vec{\nabla}p_v + \vec{\nabla}p_i)], \tag{8}$$

where k_1, k_2, k_3, and k_4 represent diffusivities:

$$k_1 = \frac{C_2 D^0_{v,i} K_v}{C_2 D^0_{v,i} + K_{mx}(p_v + p_i)}, \tag{9}$$

$$k_3 = \frac{C_2 D^0_{v,i} K_i}{C_2 D^0_{v,i} + K_{mx}(p_v + p_i)}, \tag{10}$$

$$k_2 = k_4 = \frac{K_v K_i}{C_2 D^0_{v,i} + K_{mx}(p_v + p_i)} + \frac{C_{01}}{\mu_{mx}}, \tag{11}$$

$$K_v = C_1\sqrt{\frac{RT}{M_v}}, \tag{12}$$

$$K_i = C_1\sqrt{\frac{RT}{M_i}}, \tag{13}$$

$$K_{mx} = \frac{p_v}{p_v + p_i}K_v + \frac{p_i}{p_v + p_i}K_i, \tag{14}$$

$$D^0_{v,i} = D_{v,i}(p_v + p_i). \tag{15}$$

The desorption process takes place in the already dried region during the drying process on the surface of the porous solid structure. For the mass conservation Eq. (5) the rate of desorption has to be determined. In our case, the hyphenate kinetics model was used,

$$\frac{\partial C}{\partial t} = k_g\,(C^\star - C), \tag{16}$$

where k_g represents the mass transfer coefficient and $C^\star$ is the equilibrium water concentration. The equilibrium water concentration can be written in the following form (Ravnik et al., 2018):

$$C^\star = 0.01\exp\{2.3\,[1.36 - 0.036(T - T_0)]\}, \tag{17}$$

where T_0 is the initial temperature of the frozen material.

The presented Eqs. (1)–(6) were discretized by applying the finite difference method and solved for a simplified, 1D geometrical representation of the vial filling (Ravnik et al., 2018). The central differencing scheme was used for the spatial derivatives and the backward Euler scheme was used for the temporal derivatives. The 1D approximation was chosen in order to keep the computing time as short as possible, as the final goal of developing the lyophilization model is its incorporation into a full three-dimensional (3D) model of production lyophilizers having thousands of vials (Zhu et al., 2018), with the 1D model applied separately for each of the vials.

3. BOUNDARY CONDITIONS AND MODEL PARAMETERS

To obtain the solution, appropriate boundary conditions have to be specified. The computational domain represents both the porous and the frozen part of the filling with the sublimation front in between. On the top of the computational domain, the water vapor pressure was set equal to the partial water pressure in the drying chamber $p_{v,0}$. At the sublimation front, the water vapor pressure is equal to the saturation pressure at the temperature of the interface:

$$p_v^\star = 133.32\text{Pa} \cdot \exp\left(23.9936 - \frac{2.19\Delta H_v}{T}\right). \tag{18}$$

When the primary drying stage is terminated, only the porous region exists, and at the vial bottom the water vapor flux through the vial bottom has to be zero, i.e., $\partial p_v/\partial y = 0$. Similarly, the boundary conditions for the inert gas are zero flux at the sublimation front, $\partial p_i/\partial n = 0$, and on the top of the computational domain the inert gas pressure was set equal to the inert gas partial pressure in the drying chamber $p_{i,0}$.

Because the central position of the vial on the shelf was considered the vial sidewall boundary conditions could be set as adiabatic. The 1D numerical model therefore includes two vial surfaces, where heat is supplied to the vial: the bottom and the top surface. At the top surface, the heat radiation from the upper shelf, which is partially obstructed due to the presence of the stopper, as well as from the chamber walls, governs the supplied heat flux. At the bottom, a combination of heat radiation in the gap between the vial bottom and the shelf as well as heat conduction through the gas and at the contact area with the shelf transfer heat to the vial. In order to promote sublimation of the frozen solvent, which acts as an intensive heat sink at the sublimation interface, enough heat has to be supplied to the vial filling in order to keep a nearly constant temperature in the frozen part, enabling a good control over the lyophilization process.

The overall heat flux $\dot{Q}$, transferred from the interior of the drying chamber walls and shelves to a vial, can in general be expressed as proportional to the heat transfer coefficient K_v, cross-sectional area of the vial A_v, and temperature difference between the exterior T_{sh} and the interior of the vial T_v, as follows:

$$\frac{dQ}{dt} = K_{vo} A_v (T_{\text{sh}} - T_v). \tag{19}$$

It has to be noted that the K_{vo} is an equivalent heat transfer coefficient, which in general includes contributions from all heat transfer mechanisms: conduction, radiation, and convection. The contribution of convection to the overall heat transfer is negligible, because of the low pressure employed and the resulting rarefied environment; therefore, the heat convection is not included in the specification of boundary conditions.

In order to develop a numerical model, suitable for the use in scale-up procedures and in the design space construction, models for the local K_v values have to be specified (see Fig. 1). Because different heat transfer mechanisms

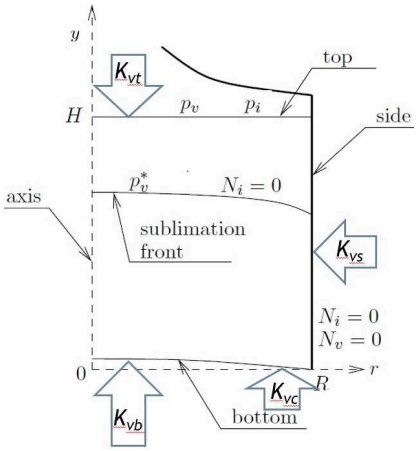

FIG. 1: Simplified vial geometry with heat transfer inputs

depend on different system parameters, each transfer mechanism has to be specified separately. In the case of heat radiation, the change in temperature of the plates directly influences the heat flux, and in the case of heat conduction through the gas phase, an increase in the system pressure leads to an increase in conduction heat transfer through the gas. Solely the contact heat conduction at the direct contact between the vial bottom and the plate remains the same for all system conditions. In the following, the models for the local K_v values, valid for the applied vial geometry, are presented.

In order to obtain the heat transfer coefficient by the contact conduction applicable to the contact area only, the K_{vc} is considered equal to

$$K_{vc} = K_{vc,\text{exp}} \frac{A_v}{A_{\text{contact}}}, \tag{20}$$

where the coefficient $K_{vc,\text{exp}}$ was set as 3.67 W/mK (Scutella et al., 2017a). The values for the contact area were determined experimentally by setting the inked vial, half filled with water, on the sheet of paper, followed by a computer analysis of the obtained image. In our case, the A_{contact} was 15.7% of the vial bottom area. In this way the K_{vc} value obtained was 23.38 W/mK.

In the gap between the plate and the vial bottom heat conduction through the gas as well as heat radiation between the two surfaces are present, i.e.,

$$K_{vb} = K_{vbr} + K_{vbc}. \tag{21}$$

The contribution from the heat radiation according to the form of Eq. (19) is set as

$$K_{vbr} = \sigma \, F_{12_b} \, (T_{\text{shelf}} + T_{\text{bot}})(T_{\text{shelf}}^2 + T_{\text{bot}}^2). \tag{22}$$

The view factor was set as

$$F_{12,b} = \frac{1}{[1 + (1/\epsilon_{\text{glass}} - 1) + (1/\epsilon_{\text{shelf}} - 1)]} \tag{23}$$

and by setting $\epsilon_{\text{glass}} = 0.78$ and $\epsilon_{\text{shelf}} = 0.18$ (Scutella et al., 2017a), we obtain

$$F_{12,b} = 0.17. \tag{24}$$

The contribution from heat conduction from the gas is (Scutella et al., 2017a)

$$\frac{1}{K_{vbc}} = \frac{1}{C_2 \, p_c} + \frac{l_b}{\lambda_{amb}} \tag{25}$$

or

$$K_{vbc} = \frac{C_2 \, p_c}{1 + (l_b/\lambda_{amb}) C_2 p_c}, \tag{26}$$

with $p_c = p_{v,0} + p_{i,0}$ the system pressure and the integral conduction length set as

$$l_b = \frac{1}{3} h_{\text{bot}}, \tag{27}$$

with h_{bot} being the maximum distance between the bottom and the plate, in our case $h_{\text{bot}} = 0.5$ mm. The parameter C_2 takes into account the free molecular flow heat transfer coefficient Λ_{o}

$$C_2 = \Lambda_{\text{o}} \left(\frac{\alpha_c}{2 - \alpha_c} \right) \left[\frac{273.15}{T_{\text{gas}}} \right]^{0.5} \tag{28}$$

with water vapor free molecular heat conductivity $\Lambda_{\text{o}} = 1,99$ [W/m^{2}Pa] and

$$\lambda_{amb} = 0.025 \text{ [W/m K]}. \tag{29}$$

The mean value of the α_c is dependent on the technical system, used for lyophilization; in our case it was set as $\alpha_c = 0.49$.

At the side wall of the vial the heat conduction through the gas as well as heat radiation between the surfaces are present, i.e.,

$$K_{vs} = K_{vsr} + K_{vsc}. \tag{30}$$

The heat conduction includes thermal heat conduction as well as the Knudsen layer conductivity (Pikal et al., 1984), in the gas phase, but since the glass wall of the vial is not included in the geometrical model, also the simplified form (parallel plates) of the contribution from the heat conduction through the side wall of the vial is accounted for, i.e.,

$$\frac{1}{K_{vsc}} = \frac{1}{C_2 p_c} + \frac{l_{ss}}{\lambda_{amb}} + \frac{\delta_{\text{glass}}}{\lambda_{\text{glass}}} \tag{31}$$

with the integral conduction length set as

$$l_{ss} = \frac{1}{3} h_{\text{fill}} \tag{32}$$

and

$$\delta_{\text{glass}} = 0.7 \text{ [mm]}, \tag{33}$$

$$\lambda_{\text{glass}} = 1.1 \text{ [W/m K]}. \tag{34}$$

The contribution from the heat radiation, i.e., the K_{vsr} for the central position of the vial, is estimated to be close to 0, as the direct vicinity of the vial is occupied by the surrounding vials at roughly the same temperature T, therefore, the radiation temperature difference is close to zero, leading to the value of $K_{vsr} = 0$.

At the top of the vial, the heat is transferred through the radiation and through conduction mechanisms:

$$K_{vt} = K_{vtr} + K_{vtc}. \tag{35}$$

The radiation contribution is

$$K_{vtr} = \sigma \, F_{12,t} \, (T_{\text{shelf}} + T_{\text{top}})(T_{\text{shelf}}^2 + T_{\text{top}}^2). \tag{36}$$

Due to the presence of the rubber stopper, obstructing the direct heat radiation from the top shelf, the value of the view factor was set as (Scutella et al., 2017b)

$$F_{12,t} = 0.12. \tag{37}$$

The contribution of heat conductivity through the gas is

$$K_{vtc} = \frac{C_2 p_c}{1 + (l_{\text{t}}/\lambda_{amb}) C_2 \, p_c} \tag{38}$$

with

$$l_{\text{t}} = h_{\text{dist}} - h_{\text{vial1}}. \tag{39}$$

For the case of the applied vial the values were $h_{\text{dist}} = 73$ mm and $h_{\text{vial1}} = 26$ mm, resulting in

$$l_{\text{t}} = 47 \text{ mm}. \tag{40}$$

Based on these models the heat transfer coefficient for the top surface was calculated as $K_{vt} = 0.91$ W/m^{2}K at the central position of the shelf. At the vial bottom, the heat transfer conditions were calculated as $K_{vb} = 9.52$ W/m^{2}K. The value of the side wall heat transfer was $K_{vs} = 4.55$ W/m^{2}K for the frozen part and $K_{vs} = 0.91$ W/m^{2}K for the porous (dry) part of the filling. Since the final part of the primary drying, when all the ice is removed, is included in the computation, the heat transfer conditions at the bottom of the vial must change, as the ice/glass contact is now replaced by porous cake/glass contact; therefore, a significant drop in heat transfer occurs. In the model, the value of $K_{vb} = 1$ W/m^{2}K was set, although a more detailed study on the value of this parameter should be made in the case of including also the secondary drying phase into the computations. Finally, the obtained overall heat transfer coefficient value K_{vo} (Eq. 19) was 15.1 W/m^{2}K.

The initial conditions for the temperature were taken to be $T_0 = 228$ K. The system pressure in the lyophilization chamber, applied at the experimental tests, was set at 12 Pa. The corresponding boundary conditions for species transport equations were calculated based on the findings of Pikal et al. (1984), where a water vapor mass fraction of 0.85 was found to be established during the primary drying; hence, the partial pressure of the water vapor was set as $p_{v,0} = 10.2$ Pa and of inert gas $p_{i,0} = 1.8$ Pa. The initial total pressure in the dried region is then $p_c = p_{i,0} + p_{v,0} = 12$ Pa, which is equal to the system pressure.

The general model parameters are summarized in Table 1.

The Table 2 lists the formulation specific material properties. In our previous research (Ravnik et al., 2018), the dependence of the drying kinetics on the Knudsen diffusivity parameter C_1 was reported. Because there is a difference in the crystal size for the mannitol and the lactose cake with the latter forming larger crystals, hence promoting the vapor diffusivity in the dried porous part of the filling, this should be reflected in the value of the C_1 (Table 2), which depends on the average pore size (Ravnik et al., 2018). As can be seen from the Table 2, a 20% lower value of C_1 was assigned in the case of the mannitol than in the case of the lactose. An in-depth study based on an extensive analysis of SEM data of the final cake porous structure would further help to improve the value of this parameter.

The heat conduction of the porous cake was computed based on the porosity value as

$$\lambda_1 = \epsilon\lambda_{\text{gas}} + (1.0 - \epsilon)\lambda_{\text{solid}} \tag{41}$$

with

$$\lambda_{\text{gas}} = 680[12.98 \cdot 10^{-8}(p_i + p_v) + 39.806 \cdot 10^{-6}]. \tag{42}$$

4. EXPERIMENTAL STUDY

All the experimental runs were made in a laboratory size lyophilizer, Christ-Epsilon 2-6, with three shelves. The freeze-drying chamber was loaded with 115 vials on each of the three shelves. The Nuova Ompi DIN ISO 10R borosilicate glass vial, with 22 mm of the outer diameter and 1 mm of glass thickness, was used in the experiments.

TABLE 1: Value of different variables in the lyophilization model

Variable	Value or model
C_{01} [m^2] Song and Nam (2005)	$7.219 \cdot 10^{-15}$
C_2 Mascarenhas et al. (1997)	0.4428
C^* Mascarenhas et al. (1997)	$0.01 \exp 2.3[1.36 - 0.036(T - T_0)]$
$c_{p,g}$ [J/kgK]	1674.7
$D^0_{v,i}$ [kg/ms^3] Song and Nam (2005)	$0.00014931[T^3(1/M_v + 1/M_i)]^{0.5}$
ϵ	0.95
h_{fill}	11.5 mm
ΔH_v [kJ/kg] Sheehan and Liapis (1998)	2840.2
ΔH_s [kJ/kg] Sheehan and Liapis (1998)	2687.4
k_g [s^{-1}] Mascarenhas et al. (1997)	$11.08 \cdot 10^{-5}$
k_2, k_4	0
k_b [m^2 kg s^{-2} K^{-1}]	$1.38064852 \cdot 10^{-23}$
M_i [kg/kmol]	29
M_v [kg/kmol]	18
μ_{mx} [kg/ms] Song and Nam (2005)	$18.4858[T^{1.5}/(T + 650)]$
$p_v^\star$ [Pa] Mascarenhas et al. (1997)	$133.32 \cdot \exp(23.9936 - 2.19\Delta H_v/T)$

TABLE 2: Material properties of lactose and mannitol

Parameter	Lactose	Mannitol
C_1 [m]	$9 \cdot 10^{-6}$	$7 \cdot 10^{-6}$
$c_{p,1}$ [J/kgK]	1650	1715
$c_{p,2}$ [J/kgK]	1893	2054
λ_{solid} [W/m K]	0.118	0.101
λ_1 [W/m K]	Eq. (41)	Eq. (41)
λ_2 [W/m K]	2.806	2.661
ρ_{solid} [kg/m^3]	1589.6	1500
$\rho_{1,p}$ [kg/m^3]	79.48	75.0
ρ_2 [kg/m^3]	957.3	952.8
ρ_1 [kg/m^3]	263	260

The vials were filled with 4 mL of the 5 wt% aqueous mannitol solution for the first set and 4 mL of the 6 wt% aqueous lactose solution for the second set of experiments. The selected vial positions were the center vials placed on the middle shelf of the lyophilizer. The temperatures of the product and the walls were measured with an external measuring system comprised of thermocouples type T, a data acquisition unit (Agilent 34970A and 34901A) and a personal computer (Sitar et al., 2018). The absolute expected uncertainty of the temperature measurements was $\pm$ 2°C at the 95% confidence level, employing the coverage factor of 2 in the temperature range from -45°C to $+50$°C. The temperatures of the product inside the vials were measured at three locations along the axis of the vial: 1.5, 5, and 8.5 mm from the vial's bottom. In order to ensure a precise vertical height of the sensor position, a dedicated thermocouple holder was inserted into the vial to enable a more precise and repeatable positioning of all thermocouples.

The lyophilization protocol was as follows: decrease of the shelf temperature (5°C to -45°C, 1 h 40 min at 1 bar), freezing step (4 h at 1 bar and -45°C), pressure decrease (1 bar to 0.120 mbar, 10 min at -45°C), increase of the shelf temperature (-45°C to -18°C, 54 min), primary drying (52 h), pressure decrease (0.120 mbar to 0.050 mbar, 10 min at -18°C), increase of the shelf temperature (-18°C to 40°C, 1 h 56 min), and secondary drying (16 h).

The experimental results for the temporal change of the sublimation height position are presented in Fig. 5 for the lactose solution and in Fig. 6 for the case of mannitol solution. The essential difference between the kinetics of drying for lactose and mannitol can be explained from the experimental results of temperature histories at different positions in the frozen material for the primary drying stage. In the case of the lactose solution, we have a significant decrease in the temperature of the frozen material along almost the entire duration of the primary phase, with respect to the lyophilization of the mannitol solution. This is especially significant in the final phase of the primary drying when the sublimation of the remaining ice at the bottom of the vial is taking place. There is no such decrease in the case of drying of the mannitol solution, where the temperature of the frozen filling gradually increases throughout the duration of the primary stage. The reason for this behavior can be found after close inspection of the final, dried cake. In the case of the mannitol, the cake occupies the entire initial volume of vial filling, without any visible gaps between the porous cake structure and the vial side glass. In the case of the lactose, the porous cake exhibits strong shrinkage effect, as depicted in Fig. 2. A loss of direct contact of the filling cake with the sidewall occurs, which reduces the heat input to the frozen material, but on the other hand, increases the effective outlet area for the sublimation vapors. Because the sublimation process is driven by the pressure difference between the saturation pressure at the sublimation front, which depends primarily on the temperature level, and the vapor partial pressure in the drying chamber, the additional increase in the outer cake area, exposed to the interior of the vial, facilitates the higher sublimation rates for the case of lactose, as can be depicted from Fig. 7 showing the interface position movement for both cases. The sublimation energy, supplied from the shelf by all considered heat transfer mechanisms, for the case of lactose, can not cover the entire consumed sublimation energy, resulting in a lower primary phase temperature levels compared to the mannitol case.

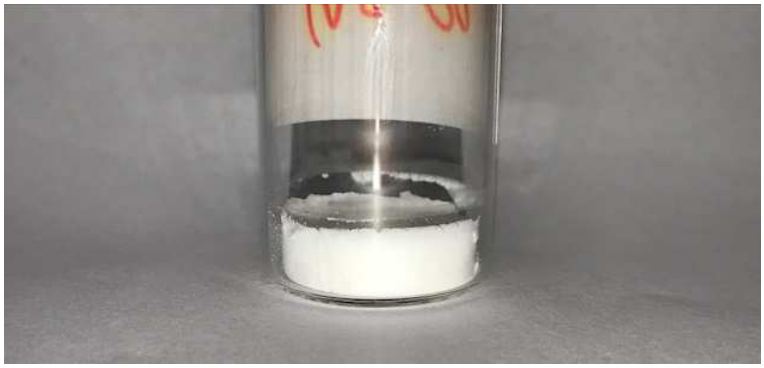

FIG. 2: Lactose cake with visible shrinkage effect

5. COMPUTATIONAL SETUP

The computational model, derived in Section 2, was implemented for the numerical simulation of lyophilization of lactose and mannitol solutions. Because the lyophilization is a time and space dependent problem, first, grid density and time step sensitivity studies for the case of mannitol solution were performed. Several grid densities were applied, from 50 to 150 equidistantly placed grid points, with a lower limit of 10 points per porous or frozen region. Similarly, the time step value was varied between 1 s and 10 s. After initial runs, a strong sensitivity of the computational results to the time step value for the first 1000 s of drying was established, where a value of $\Delta t = 1.0$ s had to be used to obtain numerically stable solutions. For the remaining part of the primary stage a much larger time step value could be used ($\Delta t = 1000.0$ s was finally selected), also with the moderately dense computational grid (50 grid points). This computational strategy greatly reduced the needed time for obtaining the numerical results.

The boundary conditions set up, presented in Section 3, can directly be applied only for a 3D or axisymmetric vial geometry. In the case of 1D vial approximation, as used in this report, the application of the side wall heat transfer input cannot be done directly. Therefore, the computed heat transfer coefficients were first transferred to their equivalent values, defined on the basis of the outer cross-sectional area of the vial as the reference heat transfer area. Furthermore, due to the moving of the sublimation front in the porous part of the filling, the high heat conductivity of the ice is replaced by the gas conductivity, thus lowering the effective heat conduction of the porous part in relation to the frozen part of the filling. This effect was taken into account when considering the redistribution of the sidewall heat transfer to the top and the bottom heat transfer coefficients by specifying the distribution coefficient, i.e., effectively increasing the top and bottom K_v values. Since the majority of the sidewall heat transfer originates from the warm shelf, the following approximation of the side wall heat transfer coefficient was made: 90% was added to the heat transfer coefficient value at the bottom and 10% to the heat transfer coefficient value at the top, which could be justified by considering the predominant conduction heat transfer mechanism near the shelf. A detailed study of this redistribution coefficient could be made based on an additional experimental study of the temperature distribution in the radial direction. Another modification of boundary conditions was required in the case of the lactose, which exhibits the shrinkage effect. In order to account for the loss of contact and hence a decrease in the heat input, a linear decrease in the side wall heat input was applied, with the starting value of $K_{v,s}$ computed for the full cake-glass wall contact case (i.e., 4.55 W/m^{2}K) and the final side wall heat input, calculated for the total loss of cake contact with the glass side wall, equal to 1.3 W/m^{2}K.

The developed computational model allows the conjugate computation of the desorption process within the porous region during the primary drying phase. In order to find out, whether the conjugate procedure is necessary, the computation of the lactose lyophilization under ideal (no shrinkage effect) conditions was performed. In Fig. 3 the temporal evolution of the area specific mass transfer resistance R_p is presented, defined as the average value for the cross-section of the vial filling A_p by using the computed overall mass transfer rate $\dot{m}_v$, obtained by integrating the vapor mass flux rate $N_{v,n}$ over the A_p:

$$R_p = \frac{(p_v^\star - p_v)}{\dot{m}_v}. \tag{43}$$

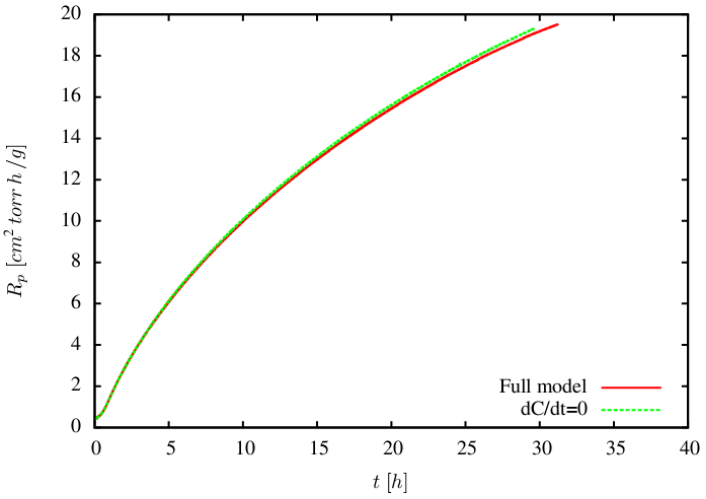

FIG. 3: Dry product resistance R_p versus time for desorption included (full model) and excluded ($dC/dt = 0$) from the primary drying phase computation

In Figs. 3 and 4 two cases are depicted: the case *Full model* stands for the computational results obtained by solving the complete lyophilization model. The case $dC/dt = 0$ stands for the case, where the desorption process was not activated when the ice was removed from the structure. In general, it is evident that the overall mass transfer resistance of the process increases with progressing of the lyophilization. At the beginning the rate of increasing is the highest and no visible differences between the active or inactive desorption are visible.

The differences become obvious towards the final stage of the primary drying phase, which can be depicted from the temporal development of the position of the sublimation interface, presented in Fig. 4, where an increase of approx. 5% in the primary drying time can be observed. This is a result of the conjugate computation of the desorption process in the porous region within the primary drying phase which increases the mass transfer resistance (see Fig. 3). The desorbed water increases the vapor pressure level inside the porous region and thus effectively decreases the pressure difference in the vicinity of the sublimation interface, thus hindering the diffusion process of the sublimated vapor. Following these findings, the desorption process was included in the computation of the primary drying phase.

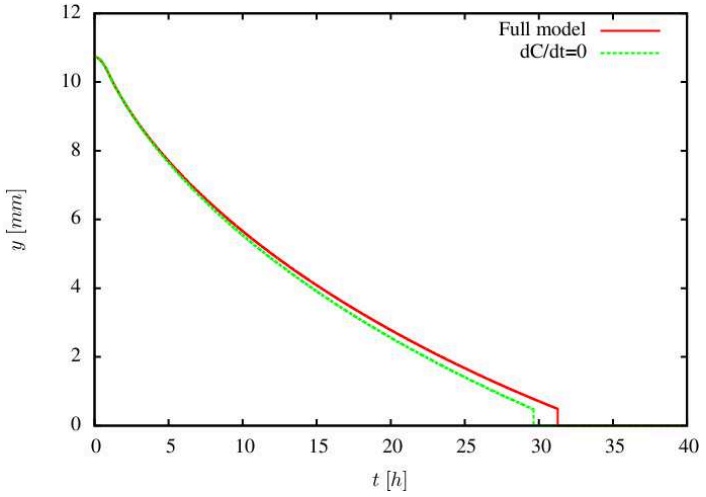

FIG. 4: Sublimation front dynamics for desorption included (full model) and excluded ($dC/dt = 0$) from the primary drying phase computation

6. COMPARISON OF EXPERIMENTAL AND NUMERICAL RESULTS

The experimental setup allowed for a continuous monitoring of the temperature at three locations inside the vial. At these three positions, an abrupt change in the temperature reading, occurring when the sublimation front has moved across a chosen sensor, served as the determination of the sublimation front position at three time instants. The fourth position, used for comparison of the experimental results with computational results, was defined as the end of the primary drying phase. As the y position for this case is 0 mm, the time instant, at which the primary phase ended, was defined as the time when all three experimental temperature readings were within 0.5 K temperature difference. Different approaches to the definition of the end of the primary drying phase to the one used in the present work were reported in Patel et al. (2010); therefore, the values from the current study should be corrected if another approach to the determination of the endpoint of the primary drying phase would be used. In order to highlight this fact, only an approximate comparison of the computed endpoint and the endpoint from the experiment are depicted in Figs. 5 and 6 for a qualitative comparison.

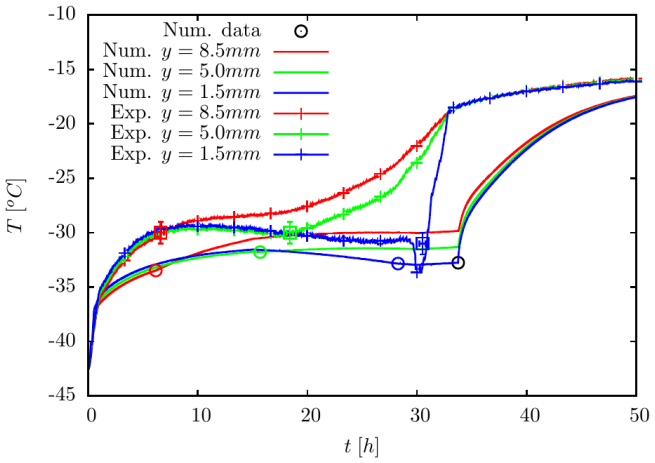

FIG. 5: Comparison of temperatures at various positions between the experimental results (thin lines) and computational results (thick lines), for the primary drying stage of lactose solution. The circles (Num. data) denote the time instants when the sublimation front passes the sensor locations with the last circle denoting the end of the primary drying.

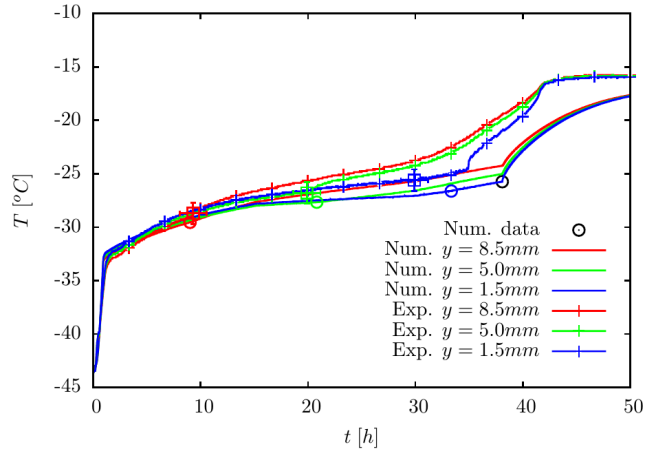

FIG. 6: Comparison of temperatures at various positions between the experimental results (thin lines) and computational results (thick lines), for the primary drying stage of mannitol solution. The circles (Num. data) denote the time instants when the sublimation front passes the sensor locations with the last circle denoting the end of the primary drying.

In Fig. 5, a comparison of drying kinetics of the lactose solution with computational results for the primary drying stage is shown. The temperature levels, obtained by the numerical simulation, are in the range of 2–4 K lower than the experimental values. The marked circular points show when the sublimation front passed a sensor location. The transition points in time at various positions in the vial filling show excellent agreement for the upper and middle thermocouple positions, whereas in the case of the third (bottom) thermocouple position still a very good agreement can be observed, all in the range of the estimated 2% error in experimental data. Also, in the numerical model, the passing of the sensor locations is reached earlier than in the experiment. The exception is the position of the endpoint of the primary drying, where the numerical result trails the experimental value.

In the case of the mannitol solution, a comparison of the drying kinetics for the primary drying stage is shown in Fig. 6. Again, the temperature levels, obtained by the numerical simulation, are approximately 1–2 K lower than the experimental values, which is a better agreement then in the case of the lactose. This was expected, as the mannitol does not exhibit cake shrinkage and the boundary conditions, used in the computational model, remain valid along the entire duration of the primary drying phase. On the other hand, the transition between the primary and secondary drying stage occurs earlier than in the experiment; however, a very good agreement in the predicted time could be observed.

The comparison of the sublimation front position inside the vial filling is depicted in Fig. 7. The agreement of the results is very good considering that the estimated 2% error in temperature values could lead to a 2 h difference in the experimental determination of the sublimation front position. In Table 3 a quantitative comparison of results for the sublimation front position is also presented, with position $y = 0.0$ mm denoting the end of the primary drying. As already stated, the agreement between numerical and experimental results is very good for all the sensor positions. In the table also a quantitative comparison of primary drying endpoints is included, as the determination of the endpoint of the primary drying is one of the most discussed topics in experimental analysis of lyophilization, Patel et al. (2010), and can lead to large differences in reported results. On the other hand, the numerical endpoint can be exactly defined as the time instant when all the ice is removed. In Table 3, the comparison of these two values, which shows a good agreement, can therefore only serve as a qualitative assessment of the accuracy of the numerical model in the primary drying endpoint determination.

7. CONCLUSION

In the present work, a comparison of experimental and computational results for the case of lyophilization of two different pharmaceutical solutions, the lactose and mannitol water solutions, was presented. The numerical model for the solution of the coupled heat and mass transfer problem in the frozen and partially dried porous part was coupled to submodels of the boundary conditions, governed by the shelf temperature and system pressure as the main process

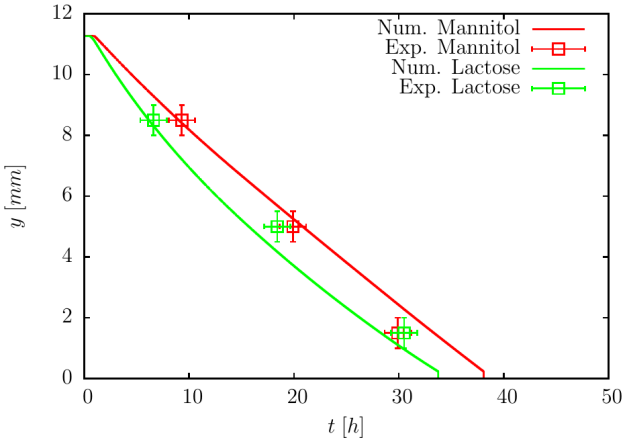

FIG. 7: Numerical results for the interface position movement within the primary drying stage

TABLE 3: Comparison of the results for sublimation front dynamics position at characteristic points

Mannitol				
Height	**Time [h]**		**Temperature [°C]**	
y **[mm]**	**Exp.**	**Num.**	**Exp.**	**Num.**
8.5	9.3 ± 1.2	9.01	-28.7 ± 1.0	-29.54
5.0	19.9 ± 1.2	20.82	-26.8 ± 1.0	-27.66
1.5	29.9 ± 1.2	33.33	-25.6 ± 1.0	-26.72
0.0	appr. 42	38.09	—	-24.70
Lactose				
Height	**Time [h]**		**Temperature [°C]**	
y **[mm]**	**Exp.**	**Num.**	**Exp.**	**Num.**
8.5	6.6 ± 1.2	6.15	-30.0 ± 1.0	-33.52
5.0	18.4 ± 1.2	15.67	-30.0 ± 1.0	-31.69
1.5	30.5 ± 1.2	28.23	-31.0 ± 1.0	-32.98
0.0	appr. 32	33.83	—	-32.77

parameters. The derived boundary conditions, valid for an axisymmetrical vial geometry, were transferred into their equivalent values, defined on the basis of the vial outer cross-sectional area, and then redistributed to the top and the bottom of the computational domain of the 1D vial approximation. In performed experiments, for the case of the lactose solution shrinkage of the cake during the primary drying was observed, leading to the occurrence of a gap between the vial wall and the cake. This effect was introduced into the model by a linear decrease of the side wall heat transfer value during the primary drying phase. The reported computational results show that the derived 1D numerical model is capable of accurately capturing the lyophilization dynamics inside a vial, and is hence suitable for the use as a vial submodel in the context of a 3D-CFD model of the lyophilization process in the lyophilizer drying chamber.

REFERENCES

Cornu, O., Banse, X., Docquier, P.L., Luyckx, S., and Delloye, C., Effect of Freeze-Drying and Gamma Irradiation on the Mechanical Properties of Human Cancellous Bone, *J. Orthopaedic Res.*, vol. **18**, no. 3, pp. 426–431, 2000.

Gan, K.H., Bruttini, R., Crosser, O.K., and Liapis, A.I., Heating Policies during the Primary and Secondary Drying Stages of the Lyophilization Process in Vials: Effects of the Arrangement of Vials in Clusters of Square and Hexagonal Arrays on Trays, *Drying Tech.*, vol. **22**, no. 7, pp. 1539–1575, 2004.

Giordano, A., Barresi, A.A., and Fissore, D., On the Use of Mathematical Models to Build the Design Space for the Primary Drying Phase of a Pharmaceutical Lyophilization Process, *J. Pharm. Sci.*, vol. **100**, pp. 311–324, 2011.

Kasper, J.C., Winter, G., and Friess, W., Recent Advances and Further Challenges in Lyophilization, *Eur. J. Pharm. Biopharm.*, vol. **85**, pp. 162–169, 2013.

Mascarenhas, W., Akay, H., and Pikal, M., A Computational Model for Finite Element Analysis of the Freeze-Drying Process, *Comp. Meth. App. Mech. Eng.*, vol. **148**, no. 1, pp. 105–124, 1997.

Patel, S., Takayuki, D., and Pikal, M., Determination of End Point of Primary Drying in Freeze-Drying Process Control, *AAPS Pharm. Sci. Tech.*, vol. **11**, no. 1, pp. 73–84, 2010.

Pikal, M., Roy, M., and Shah, S., Mass and Heat Transfer in Vial Freeze-Drying of Pharmaceuticals: Role of the Vial, *J. Pharm. Sci.*, vol. **73**, no. 9, pp. 1224–1237, 1984.

Ravnik, J., Golobi, I., Sitar, A., Avanzo, M., Irman, Š, Koevar, K., Cegnar, M., Zadravec, M., Ramak, M., and Hriberek, M., Lyophilization Model of Mannitol Water Solution in a Laboratory Scale Lyophilizer, *J. Drug Delivery Sci. Tech.*, vol. **45**, pp. 28–38, 2018.

Sadikoglu, H. and Liapis, A., Mathematical Modelling of the Primary and Secondary Drying Stages of Bulk Solution Freeze-Drying in Trays: Parameter Estimation and Model Discrimination by Comparison of Theoretical Results with Experimental Data, *Drying Tech.*, vol. **15**, nos. 3-4, pp. 791–810, 1997.

Scutella, B., Passot, S., Bourles, E., Fonseca, F., and Trelea, I.C., How Vial Geometry Variability Influences Heat Transfer and Product Temperature during Freeze-Drying, *J. Pharm. Sci.*, vol. **106**, no. 3, pp. 770–778, 2017a.

Scutella, B., Plana-Fattori, A., Passot, S., Bourles, E., Fonseca, F., Flick, D., and Trelea, I., 3D Mathematical Modelling to Under-Stand Atypical Heat Transfer Observed in Vial Freeze-Drying, *App. Thermal Eng.*, no. 126, pp. 226–236, 2017b.

Sheehan, P. and Liapis, A.I., Modeling of the Primary and Secondary Drying Stages of the Freeze Drying of Pharmaceutical Products in Vials: Numerical Results Obtained from the Solution of a Dynamic and Spatially Multi-Dimensional Lyophilization Model for Different Operational Policies, *Biotech. Bioeng.*, vol. **60**, no. 6, pp. 712–728, 1998.

Sitar, A., Skrlec, K., Voglar, J., Avanzo, M., Kočevar, M., Cegnar, M., Irman, S., Ravnik, J., Hriberšek, M., and Golobič, I., The Effects of Controlled Nucleation on Freeze-Drying Lactose and Mannitol Aqueous Solutions, *Drying Tech.*, vol. **36**, pp. 1–10, 2018.

Song, C. and Nam, J., A Numerical Study on Freeze Drying Characteristics of Cylindrical Products with and without Container, *Int. J. Transp. Phenom.*, vol. **7**, no. 3, p. 241, 2005.

Zhu, T., Moussa, E.M., Witting, M., Zhou, D., Sinha, K., Hirth, M., Gastens, M., Shang, S., Nere, N., Somashekar, S.C., Alexeenko, A., and Jameel, F., Predictive Models of Lyophilization Process for Development, Scale-Up/Tech Transfer and Manufacturing, *Eur. J. Pharm. Biopharm.*, vol. **128**, pp. 363–378, 2018.